Hindawi
Advances in Materials Science and Engineering
Volume 2021, Article ID 9582421, 10 pages
https://doi.org/10.1155/2021/9582421

Research Article

Effect of Shielding Gas on Microstructures and Mechanical Properties of TC4 Titanium Alloy Ultranarrow Gap Welded Joint by Laser Welding with Filler Wire

Naiwen Fang,[1,2] Erjun Guo ,[1] Kai Xu,[2] Ruisheng Huang,[2] Yiming Ma,[2] Caiyou Zeng,[3] Yicheng Yang,[2] Jilin Xie,[4] and Hao Cao[2]

[1]*Harbin University of Science and Technology, Harbin 150080, China*
[2]*Harbin Welding Institute Limited Company, Harbin 150028, China*
[3]*China-Ukraine E.O. Paton Institute of Welding, Guangzhou 510651, China*
[4]*Nanchang Hangkong University, Nanchang 330063, China*

Correspondence should be addressed to Erjun Guo; guoerjun98@126.com

Received 8 June 2021; Revised 2 July 2021; Accepted 19 July 2021; Published 2 August 2021

Academic Editor: Miguel Angel Torres

A 20 mm thick TC4 titanium alloy plate was welded by ultranarrow gap laser welding with filler wire with Ar and He as shielding gas, respectively. A characterization analysis of the microstructures and mechanical properties of the welded joint was conducted with OM, SEM, XRD, and EBSD and through the microhardness test and tensile test. The results showed that HAZ of the welded joint formed with Ar as shielding gas was much wider than that with He, and weld microstructure composition with the two shielding gases was basically consistent; phase boundary of the weld metal obtained with Ar was clearer, with a larger misorientation between the laths; α' martensite lath in weld metal prepared with He showed obvious preferred orientation distribution, and α' martensite microstructure was much finer; the misorientation of α' phase grain boundary of weld microstructure prepared with Ar was slightly less distributed in high angle grain boundary than that with He; tensile property of the welded joint prepared with He was better than that with Ar; the hardness of each zone of welded joint prepared with He was less fluctuated and the hardness value measured was slightly higher than that with Ar.

1. Introduction

TC4 (Ti-6Al-4V) titanium alloy is widely applied in aerospace and bathyscaph industries due to its high specific strength, low density, and good corrosion resistance [1, 2]. Titanium alloy is reactive, so it is easy to react with certain elements in air during welding, resulting in defects such as weld inclusion and crack. In the welding process of medium thickness titanium alloy plates, high-quality welded joint is hardly obtained by using common welding techniques due to the large weld filling amount and the difficulty in root protection. At present, medium thickness titanium alloy is joined mainly by magnetic controlled narrow gap TIG welding and vacuum electron beam welding [3, 4]. With magnetic controlled narrow gap TIG welding, weaknesses including high heat input and difficulty in deformation control are noticed. Electron beam welding can realize one-time welding formation, but its application is restrained by the size of welded components. Moreover, relevant equipment is expensive and may produce radiation, so this welding technique is not widely used in the formation of medium thickness and large-size components. However, in laser welding with filler wire, the heat input is low and energy can be precisely controlled. The fusion of welding wire can introduce nucleation particles to refine weld microstructure and improve the performance of the weld [5]. It is of great significance for achieving low deformation, high-quality, and high-efficiency welding of medium thickness titanium alloy components. Therefore, laser welding with filler wire will become a trend to achieve high-quality and efficient joining of titanium alloys [6].

The affinity of titanium to oxygen, nitrogen, and hydrogen is very strong at high temperature. If welded without shielding gas, titanium alloy begins to react with hydrogen at 300°C, with oxygen at 600°C, and with nitrogen at 700°C. These elements might cause joint embrittlement after their reaction with titanium alloy, resulting in the increase in hardness of welded joint and severe decrease in plasticity [7]. The thermal conductivity of titanium alloy is low, about 1/4 of nickel, 1/5 of iron, and 1/14 of aluminum. Its lower thermal conductivity leads to a longer holding time of welded joint at high temperature which prolongs its contact time with hydrogen, oxygen, and nitrogen in air and greatly increases the probability of defects in welded joint. All these factors increase the difficulty of narrow gap laser welding for titanium alloy plate with filler wire [8]. Inert gas, which is used as shielding gas during welding, can effectively prevent the contact between liquid molten pool and the air. It plays an important role in protecting high temperature weld, preventing reaction between weld and the air, and improving welding quality. At the same time, the inert shielding gas directly contacts with the molten pool. Its influence on the flow of the molten pool and the heat exchange behavior with the molten pool might greatly affect the solidification of the molten pool, therefore affecting weld quality. Scholars at home and abroad have conducted related research on the influence of shielding gas on welds. For instance, Albright et al. [9] used mixed He + Ar and CO_2 + Ar as shielding gases to study the laser-MAG arc hybrid welding for Q235 steel plate. The results showed that composition and proportion of shielding gas had obvious influence on welding performance and features of weld formation, and weld obtained with He + Ar gained larger weld penetration and greater hardness. Lu et al. [10] probed into the effect of O_2 content in Ar + O_2 mixed gas on TIG welding. When the volume fraction of O_2 increased to 0.3%, it decomposed into O atoms at high temperature and then entered the molten pool, both the surface tension and the flow direction of the molten pool were changed, and a deep and narrow weld was formed; with the addition of CO_2 and O_2, diameter of molten droplet and the threshold current of spray transfer were decreased. Duan et al. [11] found that Ar and He as shielding gases separately had different effects on the keyhole stability and metal vapor/plasma during laser welding of 5A90 Al-Li alloy. The absorption of laser energy, the flow of molten pool, and the thermal process of weld were different under the two shielding gases. Lei et al. [12] conducted research on the influence of dual-beam laser welding of 5A06 aluminum alloys with filler wire on porosity formation ratio and found that when He was used as shielding gas, plasma had little shielding effect on laser, so He is helpful in stabilizing welding process. It can be concluded from the above-mentioned research that for both laser welding and arc welding, shielding gas is a key factor affecting welding performance and property. Especially for laser welding, shielding gas is effective in eliminating plasma shielding effect, improving process stability, and realizing deep penetration welding [13, 14]. As for molten pool, shielding gas is necessary for the prevention of oxidation and pollution of the molten pool during welding at high temperature.

Therefore, how to choose appropriate shielding gas becomes a prerequisite for the investigation of laser welding of titanium alloy with filler wire. In this paper, Ar and He were used as shielding gas in laser welding of TC4 titanium alloy with filler wire, and microstructures and properties of welded joint obtained were comparatively discussed, which is expected to provide technical support for practical engineering application in future.

2. Experimental Method

2.1. Experimental Material. The dimension of TC4 titanium alloy plate used in the experiment was 300 × 150 × 20 mm. A Y-shaped groove was designed, with a root face of 2 mm, a root gap of 3 mm, and a bevel angle of 1°. An anti-deformation with a bevel angle of 1.5°was also designed. 4 supporting plates were prepared and placed under the test plate to rigidly fix it. Groove shape of the welding test plate is shown in Figure 1. The filler metal was TC3 welding wire with a diameter of 1.2 mm. The chemical composition of the base metal and filler wire is shown in Table 1. The basic physical parameters of shielding gases are given in Table 2.

2.2. Experimental Equipment. Figure 2 shows a self-designed laser welding system, consisting of a YLS-30000 fiber laser and a FLW D50W laser welding head by IPG. Its maximum output power is 12 kW. The wire feeder is Fronius KD1500D-11. The welding process was completed by the KUKA robot automatic welding system.

In the welding process, a self-made shielding gas hood was used for shielding from the underside of the test plate. By using the hood, shielding gas was introduced to the back of the test plate during the preparation of the bottom layer. Shielding gas was applied 10 s before welding to eliminate air around the surface and underside of the workpiece. Shielding gas was continuously applied for 5 s with a gas flow of 15 L/min after welding so that high temperature zones of the front and back of the weld were remain protected during the cooling process. Relative positions of laser beam, welding wire, and shielding gas are shown in Figures 3 and 4.

Before welding, the test plate was polished and then acid pickled in the solution of 5%HF + 30%HNO_3 + H_2O to remove oil and oxides from the surface. Then, the test plate was rinsed with water to wash out acid and dried for use. The laser welding process with Ar as shielding gas was completed by 1 run of laser backing autogenous welding and 9 runs of laser welding with filler wire. The laser welding process with He as shielding gas was conducted through 1 run of laser backing autogenous welding and 8 runs of laser welding with filler wire. Laser beam circular oscillation was adopted in the welding process with an amplitude of 2 mm, a frequency of 100 Hz, and a laser-wire distance of 0. Other welding parameters are shown in Table 3.

The microstructures were analyzed by using an OLYMPUS optical microscope. The grain boundary characteristics and fracture morphology of welded joints were observed by the FEI Quanta-200 field emission scanning electron microscope (FE-SEM), which was equipped with

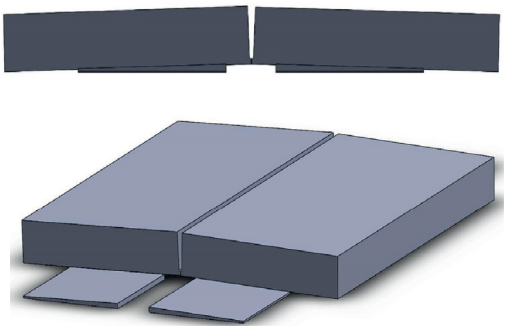

Figure 1: Shape of welding groove.

Table 1: Chemical compositions of base metal and filler metal.

Material	Al	V	Fe	C	N	H	O	Ti
TC4	6.30	4.11	0.018	0.024	0.007	0.001	0.14	Balance
TC3	4.75	3.82	0.044	0.012	0.006	0.001	0.081	Balance

Table 2: Basic physical properties of shielding gases.

Type of shielding gas	Ionization energy (eV)	Boiling point (°C)	Relative molecular mass	Density (kg/m^3)
Ar	15.76	−185.9	40	1.38
He	24.56	−268.9	4	0.14

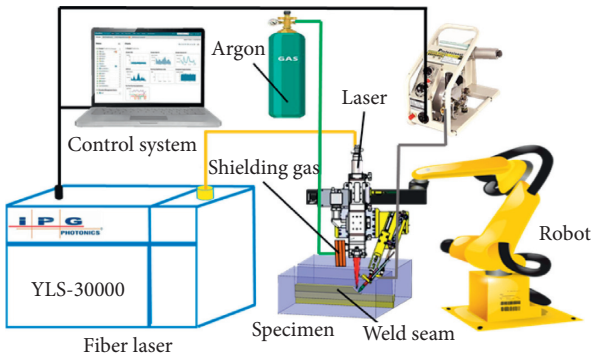

Figure 2: The system of laser welding with filler wire.

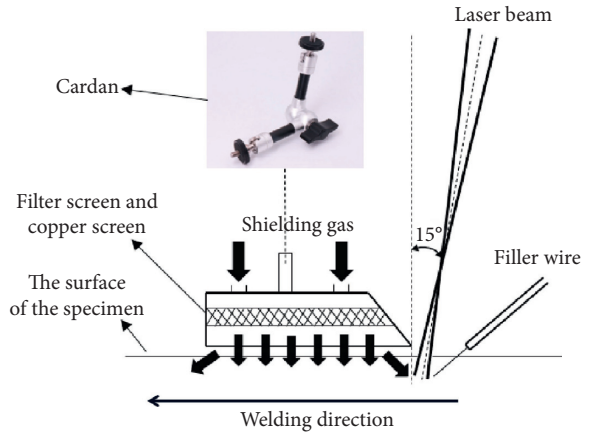

Figure 3: Experimental set-up of narrow gap laser welding.

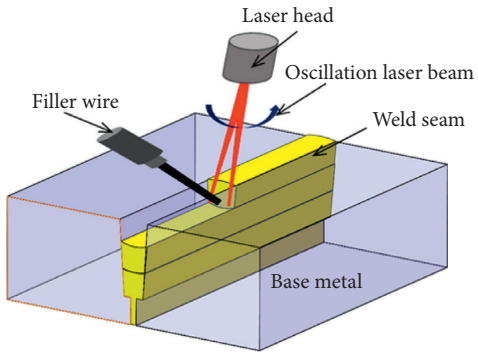

Figure 4: Schematic diagram of welding experimental equipment.

the electron backscattered diffractometer. The D/MAX-rB X-ray diffractometer was used to determine phase composition of the weld. The microhardness was analyzed by the HVS-1000Z hardness tester. The specimen for the tensile test at room temperature was prepared according to Figure 5 and tested on an INSTRON 5569 electronic universal testing machine.

3. Experimental Result and Discussion

3.1. Effect of Shielding Gas on Microstructures of Welded Joint. Figure 6 shows microstructures of welded joint obtained by using different shielding gases. It can be noticed that microstructures of TC4 titanium alloy base metal are typical equiaxed structures composed of equiaxed α phase and β phase, which are uniformly distributed. β phase is attached

Table 3: Welding parameters.

Locations	Laser power P (kW)	Welding speed V_1 (m·min^{-1})	Wire feed speed V_2 (m·min^{-1})	Defocusing amount Δf (mm)
Weld root	2.5	3	0.6	+15
Filling and capping area	3	3	0.6	+15

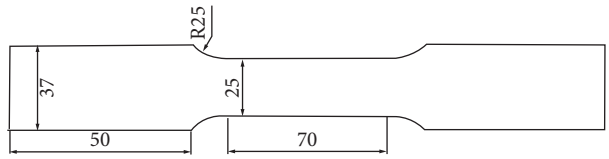

Figure 5: Schematic drawing of drawing sample processing.

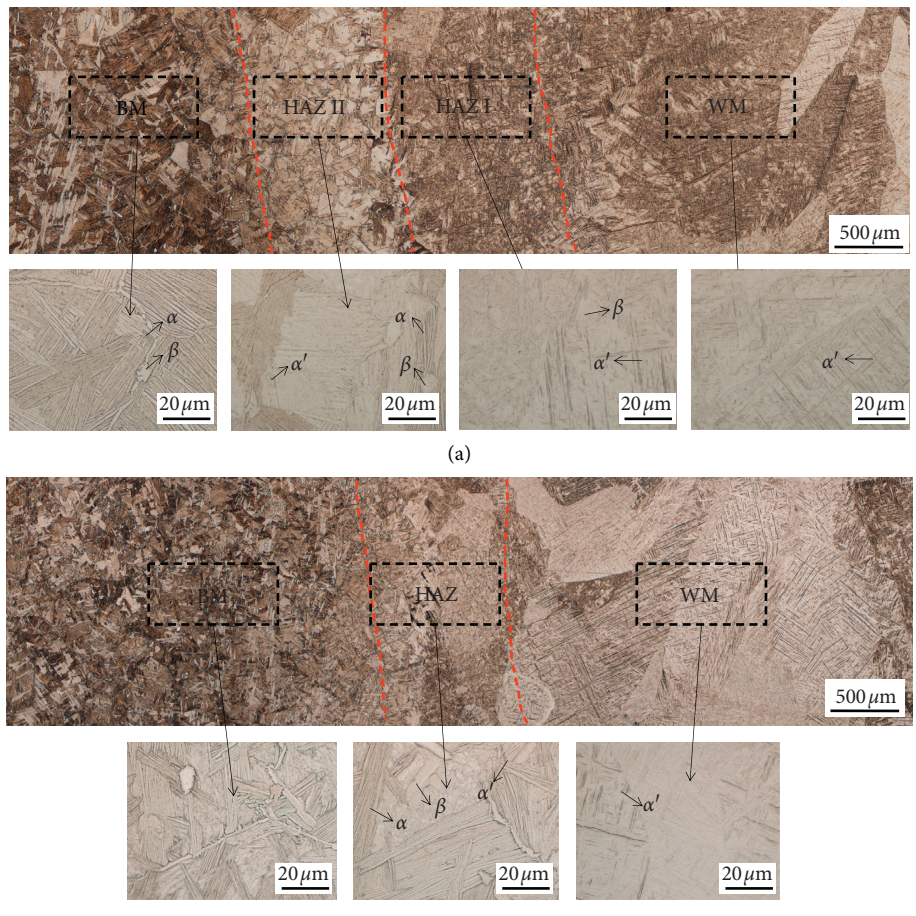

Figure 6: Microstructures of weld metals jointed with different shielding gases: (a) Ar; (b) He.

to the periphery of α phase in the matrix and evenly distributed. The microstructures of base metal in Figures 6(a) and 6(b) are basically the same. α phase content is at about 63.25%, and the average grain size is 4.25 μm. The HAZ and microstructures of welded joint are different under different shielding gases. In Figure 6(a), HAZ of the welded joint obtained with Ar as shielding gas is divided into two parts. Microstructures of HAZ I (coarse grain zone) near the weld are composed of basket-like α' phase and relatively coarse β phase. Peak temperature of the zone is close to the melting point, and its holding time at high temperature is longer. The diffusion coefficient of β phase atom above phase transformation temperature was higher, which leads to excessive grain growth. In contrast to HAZ I (coarse grain zone), HAZ II (fine grain zone) that is near the base metal has a short holding time above the phase transformation temperature.

There is not enough time for grain growth, so grains are finer. Microstructures of the zone are primary intergranular α' phase + massive α' phase + intragranular lamellar ($\alpha + \beta$). Microstructures of the zone retain the microstructure of the base metal but with blurred α phase grain boundary. The total width of the HAZ (HAZ I + HAZ II) is about 2.0 mm. The weld microstructure is composed of a single bundle of α' phases with an aspect ratio of 9.4. In the cooling process, hexagonal α' phase nucleated and grew from β phase columnar grain boundary to grain interior, forming a slender and parallel needle-like α' phase that penetrated the entire β columnar grains. The growth direction of needle-like α' phases is parallel to the optimal growth direction, and the growth rate is about 500 times that is perpendicular to the optimal growth direction [15].

Compared with Ar, He has a stronger cooling effect. Hence, holding time of the welded joint above the phase transition temperature is shorter while using He as shielding gas. Therefore, HAZ of the welded joint is composed of only one part, and the width is greatly reduced to about 0.55 mm. The time for grain growth is shorter, and the grains are finer. The final microstructure of HAZ consists of a small amount of interlaced basket-like α' phase, needle-like α phase, and relatively coarse β phase. This is because there is a certain degree of temperature gradient from the weld center to the HAZ. Under the condition of rapid cooling rate, holding time of the weld at high temperature β phase zone was relatively shorter with He as shielding gas. Only a small part of the β phase is transformed into α' phase and most of it undergoes diffused phase transformation, forming a lot of needle-like α phases, which are relatively slender due to the rapid cooling rate.

There are two kinds of phase transformation in TC4 titanium alloy weld metal during the cooling process. One is diffusion phase transformation: high temperature β phase $\longrightarrow \alpha$ phase, and the other was diffusionless transformation: high temperature β phase$\longrightarrow\alpha'$ martensite [16]. From the continuous cooling transformation (CCT) curve of titanium alloy, temperature for the transformation from high temperature β phase to α phase decreases with the increase in the cooling rate, while that of high temperature β phase to α' martensite ($Ms = 560^{\circ}C$) was not restrained by the cooling rate [17]. After undergoing thermal cycle of laser welding, the original β phase and α phase in weld microstructures are completely transformed into high temperature β phase and then began to cool down.

At the beginning of the cooling process, the heat loss and the cooling rate are fast. The high temperature β phase underwent diffusionless phase transformation. α' martensite phase diffused and nucleated in β grain and stopped at β grain boundary, forming a basket-like structure with high aspect ratio. Due to high thermal conductivity of He, it was difficult for the remaining high temperature β phase to diffuse and transform into α phase in the cooling process. The original β grain size was closely related to the holding time at high temperature. The shorter the holding time, the smaller the original β grain. The growth of long needle-like martensite α' phase was hindered, and the normal growth direction was disrupted. Eventually, short and irregularly arranged needle-like α' phases with an aspect ratio of 19.1 were formed in the weld zone.

Figure 7 shows the XRD pattern and SEM images of the weld with two types of shielding gases. From Figure 7(a), it can be found that microstructures of the weld zone are hexagonal close packed (HCP) crystal structure. Through the observation of c/a constant of each hexagonal lattice and the microstructures, it can be determined that microstructure in the weld is α' martensite, and all the main strong peaks appear while $2\theta = 40.5^{\circ}$. In the rapid cooling process of weld microstructures of titanium alloy from high temperature, crystal structure of high temperature β phase was changed, but its composition and concentration remained basically the same; thus, supersaturated solid solution, i.e., α' martensite was formed [18]. Research of relevant scholars [19] shows that the morphology, size, and lattice constant of quenched martensite are greatly related to the cooling rate. With the increase in the cooling rate, resistance to lattice reconstruction is reduced. High temperature β phase can be easily transformed into α' martensite of hexagonal lattice. α' peaks are higher in weld microstructure obtained with shielding gas He.

Figure 7(b) is the SEM image of the weld zone of welded joint obtained with Ar as shielding gas. β phase grew into coarse martensite, and α' phase without diffusion transformation was formed by direct shear during rapid cooling after the welding process. In the same martensite bundle, needle-like α' martensite monomers were in parallel and presented high-brightness and projected needle-like morphology under SEM. Figure 7(c) is the SEM image of the weld zone with He as shielding gas. Martensite α' phase was elongated needle-like and interspersed irregularly with each other in basket-like distribution. The morphology difference between the two martensitic α' phases might by caused by the fact that temperature of the molten pool exceeded $\alpha + \beta$ transformation temperature during laser welding with filler wire, and original α and original β phases were fully transformed into high temperature β phase; during the cooling process, coarse high temperature β phase grain boundary was retained, and the actual cooling rate of the weld center was faster than the critical cooling rate of α' phase; α' martensite precipitated and grew in the coarse grain boundary of β phase and inside the grain, producing supersaturated α' martensite in needle-like distribution throughout the grains; the primarily generated parallel α' phase continuously splits β phase grains, and then fine α' phases with different sizes and orientations were secondarily generated around the primary α' phase; cooling rate of the molten pool with He as shielding gas was relatively high, and the ability of secondary α' phase to further split β phase grains got stronger, so martensite bundles in different directions interlaced with each other and formed disordered microstructure.

In addition, two types of original β grain boundaries can be observed in the microstructures, which are continuous grain boundary (as shown in Figure 7(b)) and discontinuous grain boundary (as shown in Figure 7(c)). It can be concluded from analysis that with Ar as shielding gas, discontinuous grain boundary is generated, the cooling rate is

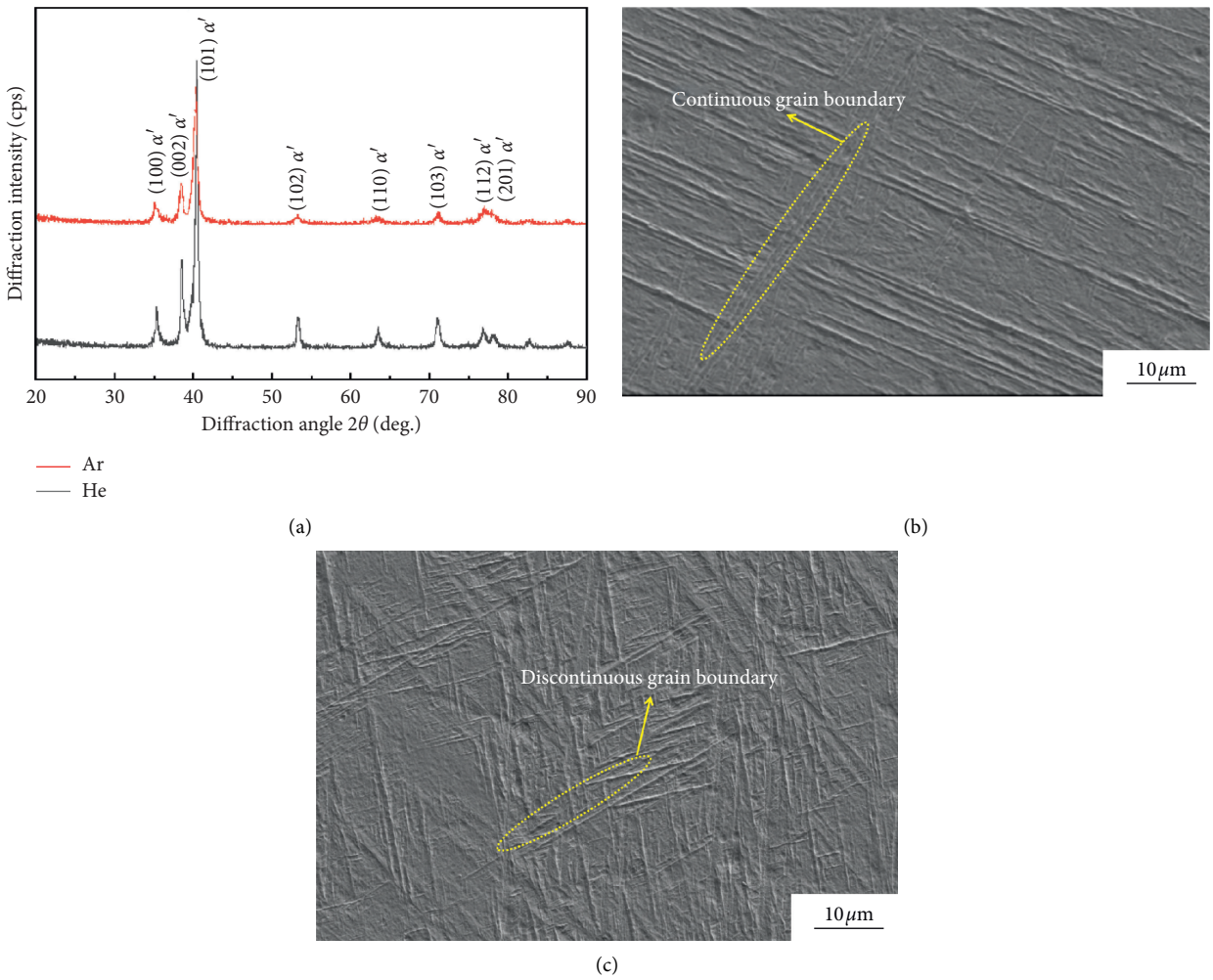

Figure 7: XRD patterns of weld zone (a) and SEM images of weld zone with different shielding gas: (b) Ar and (c) He.

slow, which results in low supercooling degree, and grain nuclei can only be produced in grain boundary and its growth is slow, so continuous grain boundary can hardly be formed; when He is used as shielding gas, the cooling rate of the weld microstructure is fast, and the supercooling degree produced is higher, so there is enough power for grain nuclei to grow rapidly and continuously.

Figures 8(a) and 8(b) are EBSD orientation imaging maps of weld metals with Ar and He as shielding gas. From the illustration of Figure 8(a), grain boundary of α' martensite in the weld zone of the welded joint obtained with Ar is clearer and the width of the fine martensite lath is about several hundred nanometers. Further observation shows that there is large orientation difference between α' martensite laths. Compared with Figure 8(b), it is found that α' martensite laths in the weld metal of the welded joint obtained with He are strip-like and show obvious preferred orientation distribution. The difference of α' martensite is mainly due to the high cooling rate of the solidification process of the molten pool obtained by laser welding of titanium alloy with filler wire. Weld metal in this condition was prone to diffusionless martensitic transformation [20], and lath martensite grew from all directions to the weld center. Molten pool prepared with He has higher cooling rate and temperature gradient compared with Ar. For weld of Ti-6Al-4V alloy, when the body-centered cubic β phase transforms into the HCP α' martensite phase, a Burgers lattice correspondence relationship between the two phases is required [21, 22], namely, $\{0001\}\alpha//\{110\}\beta$ and $<1120>\alpha//<111>\beta$. Theoretically, β phase with a specific orientation can be transformed into 12 α' martensite variants with different orientations. However, under the condition of large temperature gradient, β phase with a specific orientation tends to transform into a α' martensite variant with a preferred orientation to keep the total energy of the system to the minimum. As a result, α' martensite microstructure with referred orientation was observed in coarse original β grains in the weld with shielding gas He. The analysis result is highly consistent with the analysis of microstructures stated above.

Figures 8(c) and 8(d) show the distribution of grain boundary orientation in the weld zone of welded joint with Ar and He as shielding gas, respectively. It can be found that the peak values are concentrated at 2°, 60°, and 90°, and 60° and 90° are the two most common misorientation angles for

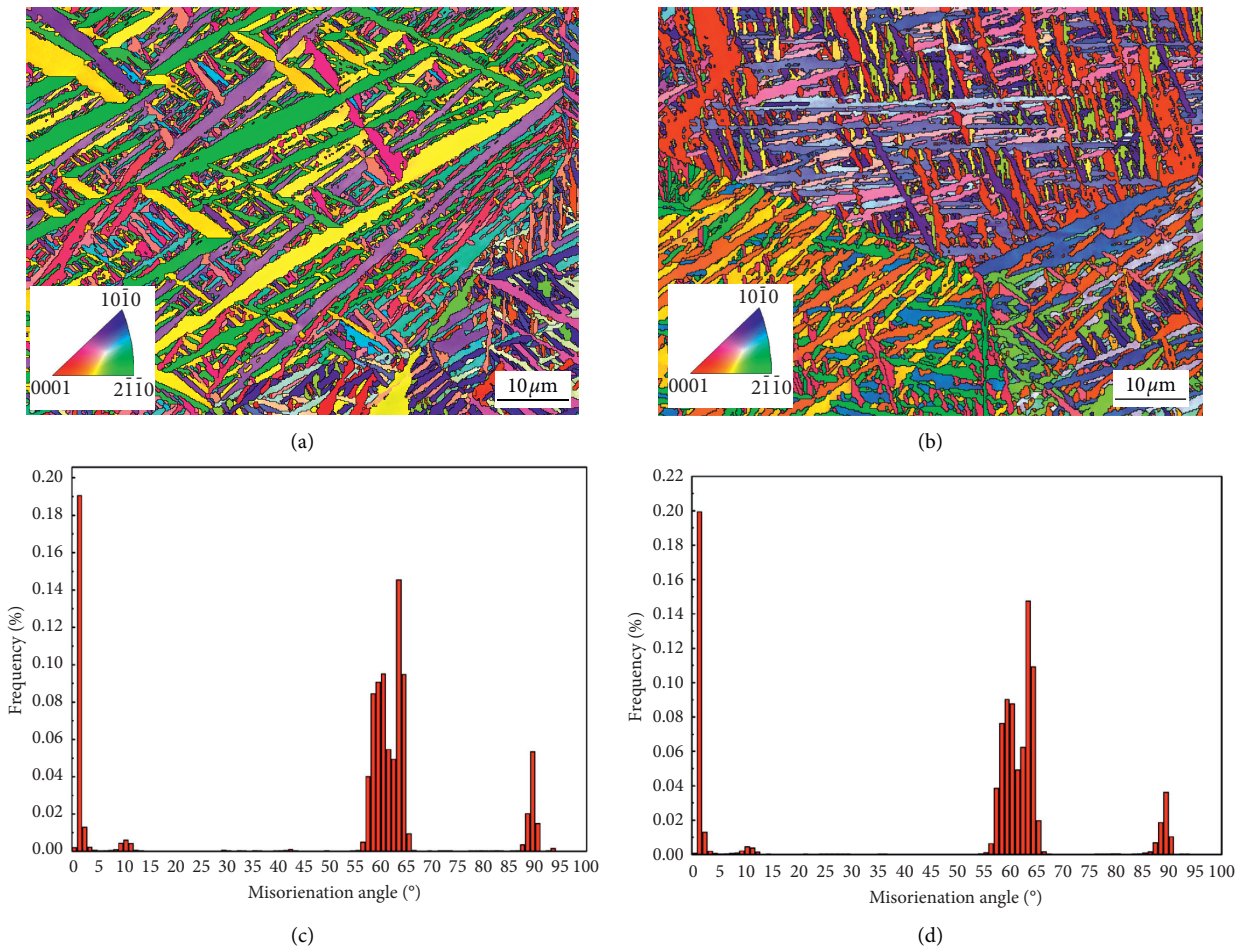

Figure 8: EBSD maps (a), (b) and the angle distribution curve of TC4 titanium alloy welded under different shielding gas states (c), (d).

α' phase transformation of titanium alloys. Usually, grain boundary with the misorientation of 2°–10° is considered as low angle grain boundary; with the misorientation of 10°–30°, it is called medium angle grain boundary; and with the misorientation ≥30°, it is named as high angle grain boundary. Grain boundary with high misorientation can effectively hinder the expansion of cleavage crack, grain boundary with medium misorientation can change the expansion direction of cleavage crack, while grain boundary with low misorientation has low energy, and dislocation structure of grain boundary is simple, so cleavage crack can easily pass through [23, 24].

According to the analysis of relevant statistics, distribution of grain boundary misorientation of α' phase in weld microstructures obtained with Ar is slightly less distributed than that with He in high angle (55°–65°) grain boundaries. The increase in high angle grain boundary helps to improve the toughness of the weld. Crack propagates in Z-shape in the grain, and it turns its direction when encountering high angle grain boundary. Crack propagation direction is related to phase difference between adjacent grains. The larger the phase difference between adjacent grains, the greater the dislocation moving resistance, the higher the crack formation angle, and thus the larger the resistance to crack propagation. Cracks turn direction when passing through high grain boundary, and the consumed energy is increased, so strength of the welded joint is improved.

3.2. Effect of Shielding Gas on the Mechanical Property of Welded Joint

3.2.1. Room-Temperature Tensile Properties. Table 4 shows data of room-temperature tensile properties of tensile specimens of TC4 titanium alloy welded joint obtained by different shielding gases. When Ar was used as shielding gas, the tensile strength was 925 MPa and the elongation was 11.5%. With He, the tensile strength of welded joint reached 931 MPa and elongation increased to 12.3%. Fracture positions under the two shielding gases are located at the fusion zone.

Figures 9(a) and 9(b) show the macromorphology of fracture surface of the welded joint and the micromorphology of central region of the macrofracture with the two shielding gases. It can be concluded that the influence of shielding gas on fracture morphology of tensile specimens of TC4 titanium alloy welded joint is obvious. With Ar as shielding gas, some shear lips can be observed in the macroscopic fracture, and the microscopic morphology of fracture is found mainly composed of shallow dimples.

Table 4: Results of tensile strength.

Type of shielding gas	Tensile strength Rm (MPa)	Yield strength Rm (MPa)	Elongation A (%)	Fracture location
Base metal	922	831	12.5	—
Ar	925	—	11.5	Fusion zone
He	931	—	12.3	

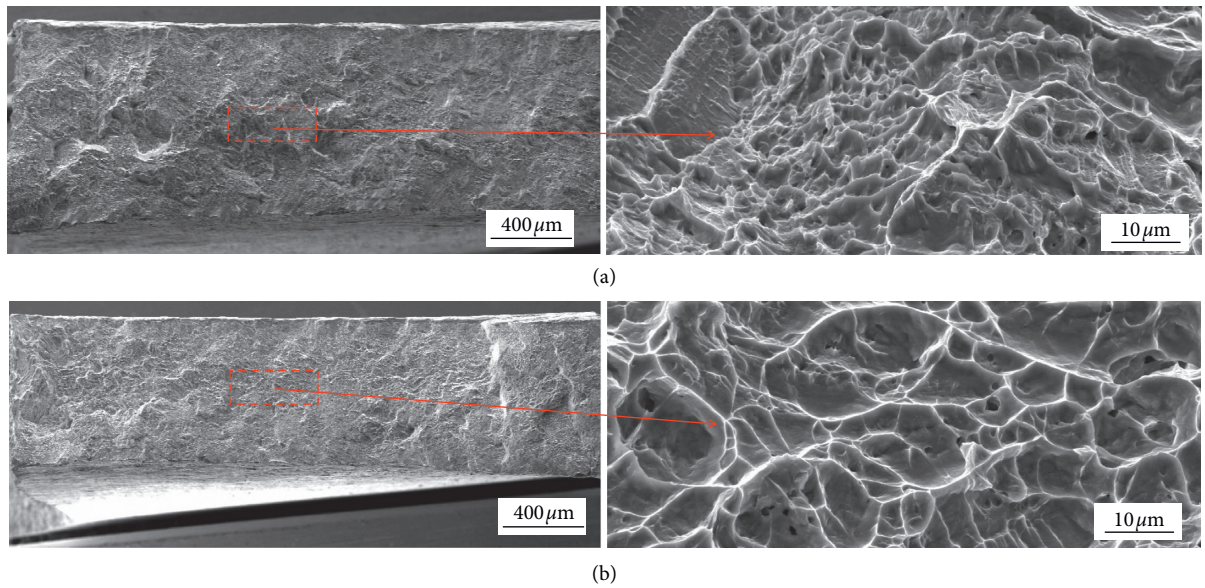

Figure 9: Fracture morphology of tensile fracture with different shielding gases: (a) Ar; (b) He.

Obvious deformation and slip can be seen in the micromorphology of fracture surface, with tear ridges occurred when breakage was generated and got unstable. Fracture steps and cleavage planes appeared at the same time, and dimples started to show on the step, indicating the fracture mechanism featured as mixed fracture. With He as shielding gas, there was a shear lip on the edge of the fracture macromorphology and obvious necking was observed. In micromorphology, there is a large area of deep dimples which are net-like connected in the fracture presenting typical transcrystalline rupture characteristics. The fracture mechanism was microvoid coalescence. At the same time, α lath became wider and more uniform, and the microstructure was typically basket-like, which increased slip distance and improved the plasticity.

3.2.2. Microhardness. Figure 10 shows the HV0.5 microhardness cloud chart of TC4 titanium alloy welded joints with different shielding gases. By comparison, it can be found that the fluctuation of hardness of the welded joint with He is relatively stable than that with Ar. During laser welding of titanium alloy, a large amount of laser-induced plasma was produced, which affected the stability of welding process and the stability of welding pool flow. The ionization potential energy of He (24.56 eV) was significantly higher than that of Ar (14.76 eV), so the effect of He on improving beam penetration was much stronger compared with that of Ar. Under certain conditions, gas with high ionization potential has a good inhibitory effect on plasma so that microstructure distribution in the welded joint is less fluctuating. Therefore, the hardness distribution of welded joint in each region is more stable with He as shielding gas.

Microhardness values of the welded joints under different shielding gases are slightly different, but the distribution trend is basically the same. The microhardness of the weld zone and HAZ with He was a little higher, and the hardness distribution of the two groups of welded joints was in the order of weld zone > HAZ > base metal. Generally, the order of hardness of each phase of titanium alloy is $\alpha' > \alpha > \beta$ [25]. Both groups of welds contained a lot of acicular martensite α' phases interlaced with each other. These α' phases had higher dislocation density and twinning, resulting in abundant phase boundaries, which makes hardness of the weld zone significantly higher than that of other regions. Moreover, a small amount of α' phase was found in the HAZ of the two groups of welded joints, so its hardness was also slightly higher than $\alpha + \beta$ phase of the base metal.

According to Hall–Petch formula, the smaller the grain size at room temperature, the more grain boundaries per unit volume, and the better the strengthening effect [26]. Hence, the finer the grain, the higher the hardness value. It can be seen from the above analysis that microstructures of the weld center obtained with He are finer than those with Ar, so its hardness is better. The microhardness peaks of the two groups of welded joints appeared in the fusion zone near the fusion line, and the microhardness decreased significantly after crossing the fusion line.

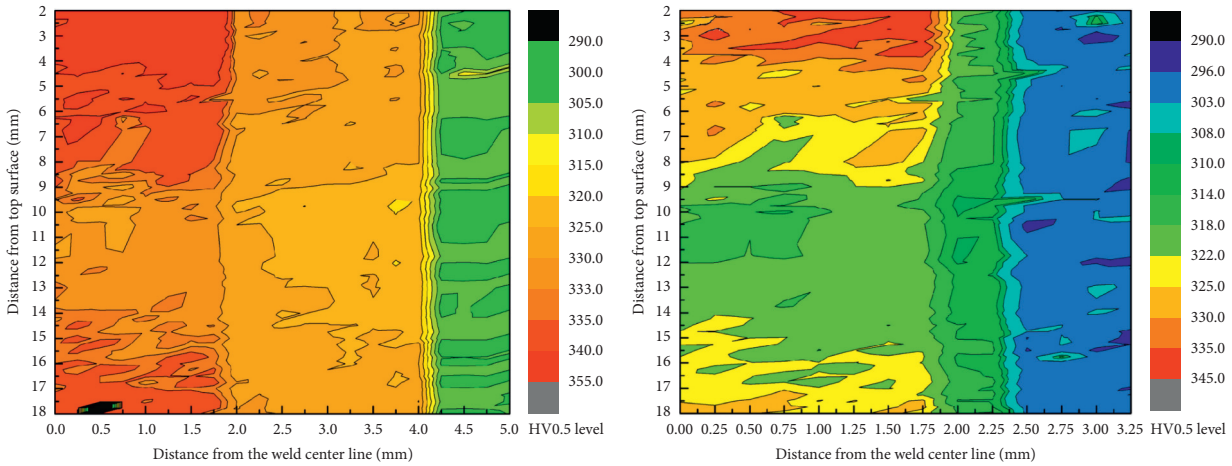

Figure 10: Microhardness distribution of weld metals jointed with different shielding gases: (a) Ar; (b) He.

Comparing with the weld center, hardness of the filling layer and the backing layer was not much different but hardness of the cover layer was higher. From analysis of the metallographic structure of each region, it can be seen that constitutional supercooling is not sufficient enough to generate heterogeneous nucleation although heat input of narrow gap laser welding with filler wire was low and the cooling rate was fast. Fine equiaxed grains were difficult to form in the weld center, and all appear as needle-like α' martensite, so there is no fine grain strengthening mechanism. Weld microstructure of the filling layer and backing layer was evenly refined by subsequent welding thermal cycle. Martensite in the cover layer was not affected by heat treatment. The layer had a faster cooling rate, so weld metal was directly sheared by β phase to fully form α' martensite, and needle-like α' martensite inside columnar grains was denser, and the martensite strengthening phenomenon was more obvious.

4. Conclusion

(1) HAZ width of the welded joint with Ar as shielding gas was much wider than that with He, and weld microstructure obtained with the two shielding gases was completely α' martensite of HCP crystal structure, and no supercooled β phase of body-centered cubic crystal structure was observed, with the main strong peaks appeared at $2\theta = 40.5^{\circ}$. Weld metal grain boundary obtained with Ar was clear, with a large misorientation between the laths. α' martensite lath in the weld metal obtained with He showed obvious preferred orientation distribution, and the aspect ratio of α' martensite phase was larger.

(2) Grain boundaries in the weld zone of welded joint concentratedly peaked at 2°, 60°, and 90 °with shielding gas Ar and He, respectively. The misorientation of α'phase grain boundary of weld microstructure prepared with Ar was slightly less distributed than that with He in large angle (55°–65°) grain boundary.

(3) With He as shielding gas, tensile strength of the welded joint reached 931 MPa, and elongation was increased to 12.3%. The tensile property of the welded joint with He was better than that with Ar. The tensile fracture mechanism of welded joint with Ar as shielding gas was characterized by mixed fracture, while that with He was microvoid coalescence fracture.

(4) The hardness of each zone of welded joint prepared with He was less fluctuated, and the hardness value was a little higher than with Ar. The hardness distribution of the two groups of welded joints was in the order of weld zone > HAZ > base metal. The microhardness peaks of the two groups of welded joints appeared in the fusion zone near the fusion line, and the microhardness decreased significantly after crossing the fusion line.

Data Availability

The data used to support the findings of this study are available from the corresponding author upon request.

Conflicts of Interest

The authors declare that they have no conflicts of interest.

Acknowledgments

This study was supported by Heilongjiang Provincial Fund for National Project (GX18A001) and Energy Equipment Advanced Welding Technology Innovation Team Fund supported by Heilongjiang Provincial Head Talent Plan (201910312).

References

[1] H. Jin, W. Kexiang, J. Li et al., "Research development of titanium alloy in aerospace industry," *Chinese Journal of Nonferrous Metals*, vol. 25, no. 2, pp. 280–292, 2015.

[2] X. Jiang, D. Cheng, Y. Chen et al., "Superplastic deformation mechanism of acicular weld microstructure of titanium alloy," *Transactions of the China Welding Institute*, vol. 39, no. 9, pp. 65–70, 2018.

[3] Y. L. Qi, J. Deng, Q. Hong et al., "Electron beam welding laser beam welding and gas tungsten arc welding of titanium sheet," *Materials Science and Engineering A*, vol. 280, pp. 177–181, 2000.

[4] J. Zhao, H. Ding, W. Zhao, M. Huang, D. Wei, and Z. Jiang, "Modelling of the hot deformation behaviour of a titanium alloy using constitutive equations and artificial neural network," *Computational Materials Science*, vol. 92, pp. 47–56, 2014.

[5] D. Yang, X. Li, D. He et al., "Effect of minor Er and Zr on microstructure and mechanical properties of Al-Mg-Mn alloy(5083)welded joints," *Materials Science and Engineering A*, vol. 561, pp. 226–231, 2013.

[6] X. Kong, Li Fei, J. Lv et al., "Fiber laser welding of 5083 aluminum alloy with filler wire," *Chinese Journal of Lasers*, vol. 41, no. 10, pp. 87–92, 2014.

[7] P. Wattanapornphan, C. Phongphisutthinan, T. Suga, M. Mizutani, and S. Katayama, "Evolution behavior of laser welding in hybrid structure between open-cell aluminum foam and solid aluminum shell," *Welding in the World*, vol. 65, no. 2, pp. 263–274, 2021.

[8] E. Le Guen, R. Fabbro, M. Carin, F. Coste, and P. Le Masson, "Analysis of hybrid Nd:Yag laser-MAG arc welding processes," *Optics & Laser Technology*, vol. 43, no. 7, pp. 1155–1166, 2011.

[9] C. B. Albright, J. Bastman, and W. Lempert, "Low-power lasers assist arc welding," *Welding Journal*, vol. 80, no. 4, pp. 55–58, 2001.

[10] S. P. Lu, H. Fujii, K. Nogi, and T. Sato, "Effect of oxygen content in He-O2shielding gas on weld shape in ultra deep penetration TIG," *Science and Technology of Welding & Joining*, vol. 12, no. 8, pp. 689–695, 2007.

[11] A. Duan, S. Gong, and F. liu, "Influence of shielding gas on temperature field distribution during laser welding of 5A90," *Journal of Mechanical Engineering*, vol. 53, no. 16, pp. 181–189, 2017.

[12] Z. Lei, Li Ying, Y. Chen et al., "Effect of process parameters on porosity formation ratio in dual-beam laser welding of aluminum alloys with filler wire," *Transactions of the China Welding Institute*, vol. 115, no. 2, pp. 40–44, 2013.

[13] Z. Li, T. S. Srivatsan, L. I. Yan et al., "Coupling of laser with plasma arc to facilitate hybrid welding of metallic materials," *Review*, vol. 22, no. 2, pp. 384–395, 2013.

[14] H. Lei, G. Wu, and W. Chen, "Influence of shielding gas flow on welding quality for CO_2 laser welding of aluminum alloy," *Chinese Journal of Lasers*, vol. 32, no. 11, pp. 1571–1576, 2005.

[15] K. J. Song, Y. H. Wei, Z. B. Dong, X. H. Zhan, W. J. Zheng, and K. Fang, "Numerical simulation of β to α phase transformation in heat affected zone during welding of TA15 alloy," *Computational Materials Science*, vol. 72, pp. 93–100, 2013.

[16] W. Wu, G. Cheng, and H. Gao, "Microstructure transformation and mechanical properties of TC4 alloy joints welded by TIG," *Transactions of the China Welding Institute*, vol. 30, no. 7, pp. 81–84, 2009.

[17] S. Huang, Y. Ma, S. Zhang et al., "Influence of alloying elements partitioning behaviors on the microstructure and mechanical properties in α+β TitaniumAlloyl," *Acta Metallurgica Sinica*, vol. 55, no. 6, pp. 741–750, 2019.

[18] N. Fang, E. Guo, R. Huang et al., "Effect of welding heat input on microstructure and properties of TC4 titanium alloy ultra-narrow gap welded joint by laser welding with filler wire," *Materials Research Express*, vol. 8, no. 1, Article ID 016511, 2021.

[19] K. C. Wu, "Correlation of properties and microstructure in welded Ti-6Al-6V-2Sn," *Welding Journal*, vol. 60, no. 11, p. 219s, 1981.

[20] M. Zhang, F. Jia, K. Cheng et al., "Influence of quenching and tempering on microstructure and properties of welded joints of G520 martensitic steel," *Acta Metallurgica Sinica*, vol. 55, no. 11, pp. 1379–1387, 2019.

[21] P.-q. Xu, L. Li, and C. Zhang, "Microstructure characterization of laser welded Ti-6Al-4V fusion zones," *Materials Characterization*, vol. 87, pp. 179–185, 2014.

[22] C. Pandey, M. M. Mahapatra, P. Kumar, F. Daniel, and B. Adhithan, "Softening mechanism of P91 steel weldments using heat treatments," *Archives of Civil and Mechanical Engineering*, vol. 19, no. 2, pp. 297–310, 2019.

[23] N. Saini, C. Pandey, M. M. Mahapatra, H. K. Narang, R. S. Mulik, and P. Kumar, "A comparative study of ductile-brittle transition behavior and fractography of P91 and P92 steel," *Engineering Failure Analysis*, vol. 81, pp. 245–253, 2017.

[24] H. Yu, F. Li, J. Yang, J. Shao, Z. Wang, and X. Zeng, "Investigation on laser welding of selective laser melted Ti-6Al-4V parts: w microstructure and mechanical properties," *Materials Science and Engineering: A*, vol. 712, pp. 20–27, 2018.

[25] T. Jibin, M. Jose, and K. Basi, "Tribology of Ti6Al4V:A review," *Friction*, no. 6, pp. 497–536, 2019.

[26] C. Y. Cui, X. G. Cui, X. D. Ren, T. T. Liu, J. D. Hu, and Y. M. Wang, "Microstructure and microhardness of fiber laser butt welded joint of stainless steel plates," *Materials & Design*, vol. 49, pp. 761–765, 2013.